College of Pharmaceutical Science[1], Zhejiang Chinese Medical University, Hangzhou; College of Pharmacy & Key Laboratory of Pharmaceutical Quality Control of Hebei Province[2], Hebei University, Baoding, PR China; Department of Oncologic Pathology[3], Harvard University Dana-Farber Harvard Cancer Center, Boston, USA; Guiyang University of Chinese Medicine[4], Guiyang, PR China

Intranasal administration of pullulan-based nanoparticles for enhanced delivery of adriamycin into the brain: *in vitro* and *in vivo* evaluation

Jiazhen Zhu[1,#], Jiafeng Zou[1,#], Chaofeng Mu[1], Wenzhi Yang[2], Mancang Gu[3], Jinmin Lin[1], Xinli Song[4], Hongyue Zheng[1], Fanzhu Li[1,*]

Received June 28, 2018, accepted September 19, 2018

[*]*Corresponding author: Fanzhu Li, Ph.D., College of Pharmaceutical Science, Zhejiang Chinese Medical University, Gaoke Road, Fuyang District, Hangzhou, 311402, PR China*
lifanzhu@zcmu.edu.cn
[#]*These authors contributed equally to this work.*

Pharmazie 74: 39–46 (2019) *doi: 10.1691/ph.2019.8124*

Intranasal (i.n.) administration is an efficient route for enhancing drug delivery to the brain, bypassing the blood-brain barrier (BBB) and eliminating systemic side effects. The purpose of this study was to investigate the nose-to-brain delivery efficiency of adriamycin (ADM) loaded in cholesterol-modified pullulan self-assembled nanoparticles (CHSP-SAN) via i.n. administration. The prepared nanodrugs (ADM-CHSP-SAN) were characterized as uniform size (112.8±1.02 nm), high drug loading capacity (7.65±0.58 %), and sustained release. CHSP-SAN showed good biocompatibility and low toxicity on HBMEC and C6 cells. The enhanced delivery of ADM across the BBB with CHSP-SAN was demonstrated by the reduced half maximal inhibitory concentration (IC_{50}) value and the increased apoptosis proportion of C6 cells. The pharmacokinetics of ADM-CHSP-SAN was accessed by cerebral microdialysis technique. The pharmacokinetic results showed higher peak concentration (C_{max}), area under the curve ($AUC_{0\text{-}12h}$) and shorter peak time (T_{max}) after i.n. administration that after intravenous (i.v.) administration. The i.n. administration of CHSP-SAN greatly increased ADM availability in cerebral tissue compared to that of ADM solution. Collectively, CHSP-SAN strikingly increased ADM transport across the BBB and improved its availability in brain via i.n. administration.

1. Introduction

Drug delivery to the central nervous system (CNS) remains highly challenging despite an improved understanding of CNS disease pathologies and etiologies as well as the identification of new targets (De Lange 2013; Potter 2012). Specifically, the presence of the blood–brain barrier (BBB), which features tight continuous circumferential junctions between the human brain micro-vessel endothelial cells (HBMEC), is a main hurdle for brain drug delivery. BBB hinders small molecule drugs and water-soluble molecules being delivered from the circulation system into the brain (Pardridge 2005). Routine approaches applied for the enhancement of drug concentrations in the brain involve craniotomy-based drug delivery, such as intraventricular drug diffusion, local intracerebral implants, or disruption of the BBB by infusion of hyperosmotic solutions and vasoactive agents prior to systemic drug administration (Babu et al. 2011). These highly invasive approaches are mostly appropriate for short-term treatments, where a single or infrequent exposure to a drug is required (Gloor et al. 2001), but are not suitable for long-term treatments.

Due to the formidable obstacle imposed by the BBB, there has been increased interest in developing new strategies to overcome the BBB. Intranasal (i.n.) administration has been implicated as a safe, non-invasive and acceptable nose-to-brain drug delivery route, especially for substances with biological effects on the CNS and limited BBB permeability (Illum 2000, 2002). Our previous study has shown that peptides, such as neurotoxin, could be transported into the brain through nose-to-brain route more efficiently than by the intravenous (i.v.) route (Li et al. 2007). The amount of drug transported into the brain could be further mediated by nanoparticles through nose-to-brain route (Cheng et al. 2008). However, conventional drug delivery systems (DDS), such as organic synthetic micelle-based and silica-based DDS, are inherently toxic and non-biodegradable. Most of them may have significant side effects and lead to irreversible damage to CNS (Bharali et al. 2005; Zhang et al. 2013). Nowadays, a variety of nontoxic and biodegradable biopolymers have been used as amphiphilic biomaterials for drug delivery. Cholesterol-modified pullulan (CHSP), which always forms self-assembled nanoparticles (SAN) embodying a hydrophobic core with cholesterol moiety and hydrophilic surface with pullulan chain, can be used as a nanocarrier for hydrophobic drugs and biomacromolecules such as peptides and genes (Rekha and Sharma 2011; Zhang et al. 2011). In our previous study, CHSP, with a degree of substitution of 5.20 cholesterol residues per 100 glucose units in pullulan, has been successfully synthesized and characterized with FT-IR spectroscopy, ^{1}H NMR spectra and DSC (Fig. 1). It has also shown high drug loading capacity, good storage stability, low toxicity and excellent biocompatibility *in vitro* and *in vivo* (Shen et al. 2014). Biodegradability is considered a mandatory feature of biomaterials for brain drug delivery. It is suggested that cholesterol-modified pullulan self-assembled nanoparticles (CHSP-SAN) may be an ideal nose-to-brain delivery carrier system. However, nasal-brain pathway drug delivery transported by the CHSP-SAN has not yet been reported.

Adriamycin (ADM), an FDA approved antineoplastic agent, demonstrated high anti-glioma activity in cell lines and xenografts. However, clinical applications of ADM alone are limited because of its severe side effects and poor ability of crossing the BBB (Gao et al. 2016). It was reported that small molecular compounds, such as ADM, have the potential to treat neurological diseases and brain tumors after intranasal administration (Babu et al. 2011). Intranasal administration is a promising strategy to deliver drugs to the brain via the olfactory nerve tract to directly bypass the

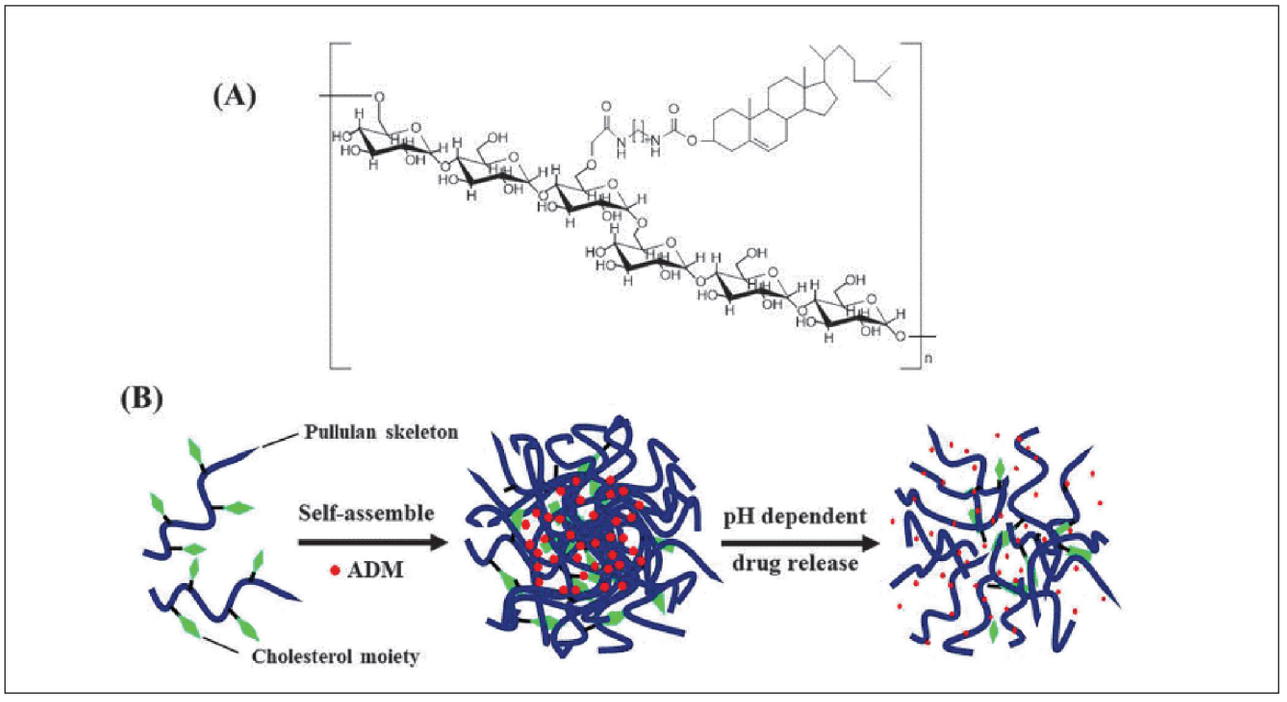

Fig. 1: Chemical structures of CHSP (A) and schematic illustration of ADM-CHSP-SAN (B).

BBB and reduce the diffusion of drugs into the blood (Hefnawy et al. 2017). The efficiency of the drug entering the brain via the nasal cavity can be further improved by encapsulation into nanocarriers (Clementino et al. 2016; Guo et al. 2017). In this study, we aimed to construct ADM loaded CHSP-SAN (ADM-CHSP-SAN) and investigated the nose-to-brain targeting delivery features of CHSP-SAN. The cytotoxicity and apoptosis of C6 cells induced by ADM-CHSP-SAN were determined with the presence of BBB *in vitro*. In addition, the brain microdialysis (B-MD) sampling technique was employed to investigate the difference of the brain pharmacokinetics (B-PK) after i.n. and i.v. administration.

2. Investigations and results

2.1. Characterization of CHSP-SAN and ADM- CHSP-SAN

Transmission electron microscope (TEM) images revealed that the morphology of CHSP-SAN and CHSP-ADM-SAN were spherical with a uniform size (Fig. 2A, B). The mean particle size, polydispersity index (PDI) and *zeta* potential of CHSP-SAN were 91.63±0.88 nm, 0.243±0.035 and 0.0040±0.0001 mV, respectively (Fig. 2C, D). The results indicated that CHSP-SAN formed an electrically neutral and good monodisperse stable system in aqueous solution. In our previous study, CHSP-SAN in aqueous media was stable for at least 2 months at 4 °C (Shen et al. 2014), which was mainly ascribed to the steric structure of pullulan-based particles (Simakov and Tsur 2007).

After loading the negatively charged drug, the *zeta* potential reversibly switched from 0.0040±0.0001 mV to -27.25±0.246 mV and the particle size slightly increased to 112.8±1.02 nm (Fig. 2E, F). In addition, the dispersion state in TEM and PDI value indicated that the loaded drug did not affect the shape and dispersibility of nanoparticles in aqueous solution. The entrapment efficiency (EE%) and drug loading capacity (DL%) of CHSP-ADM-SAN were 67.14±1.21 % and 7.65±0.58 %, respectively.

2.2. In vitro release study of ADM-CHSP-SAN

The release behaviors of ADM solution (ADM-Sol) and ADM-CHSP-SAN *in vitro* were observed in PBS (pH 7.4, pH 6.8 and pH 5.0) at 37 °C. As shown in the insert of Fig. 3, ADM was released to 96.38±1.21 %, 95.46±1.45 % and 97.10±1.15 % from ADM-Sol within the initial 2 h under three pH conditions. After ADM was loaded into CHSP-SAN, a significant reduction of *in vitro* release rate was achieved. The nanoparticles released about 30.51±2.66 %, 33.42±3.02 % and 48.25±2.25 % of drug within the initial 4 h, respectively. This showed that ADM-CHSP-SAN had sustained release characteristics. As shown in Fig. 3, a burst release was observed in the first 8 h, in which 38.5±2.56 %, 41.3±2.85 % and 59.3±3.14 % of drug was released from the nanoparticles at pH 7.4, pH 6.8 and pH 5.0, respectively. This suggested that some amount of drug may be absorbed onto the surface of nanoparticles, and therefore diffused rapidly into the release medium. After this period, ADM released in a continuous way up to 48 h, the cumulative release amount of ADM from CHSP-SAN could reach 74.76±2.15 % at pH 5.0, while only about 54.25±2.02 % and 57.82±2.23 % of ADM was released at pH 7.4 and pH 6.8, respectively. This was ascribed to the diffusion of the entrapped drug from nanoparticles. The drug release of ADM-CHSP-SAN indicated sustained release manner and best fitted the Weibull release kinetic model (Table 1), which indicated the ADM release from nanocarriers with matrix type (Carlan et al. 2017; Meng et al. 2016).

2.3. In vitro cytotoxicity assay

To evaluate the biocompatibility of CHSP-SAN, different concentrations of CHSP-SAN suspensions were incubated with HBMEC and C6 cells. As displayed in Fig. 4A, CHSP-SAN at a concentration below 125 μg/mL did not cause significant loss of cell viability in both HBMEC and C6 cells after incubation for 48 h, indicating the low cytotoxicity and good biocompatibility of pullulan nanocarriers. The cytotoxicity of ADM formulations in C6 cells are displayed in Fig. 4B. The results revealed a dose-dependent reduction in the percentage of cell viability after treatment with ADM-CHSP-SAN or ADM-Sol for 48 h. The IC_{50} values of ADM-Sol and ADM-CHSP-SAN in C6 cells were 2.21±0.55 μM and 6.22±1.17 μM, respectively. ADM in CHSP-SAN demonstrated a sustained release manner within 48 h *in vitro,* whereas free ADM could enter the cells immediately by passive diffusion. To determine whether ADM formulations may also affect the cell proliferation of HBMEC, a high ADM concentration (30 μM)

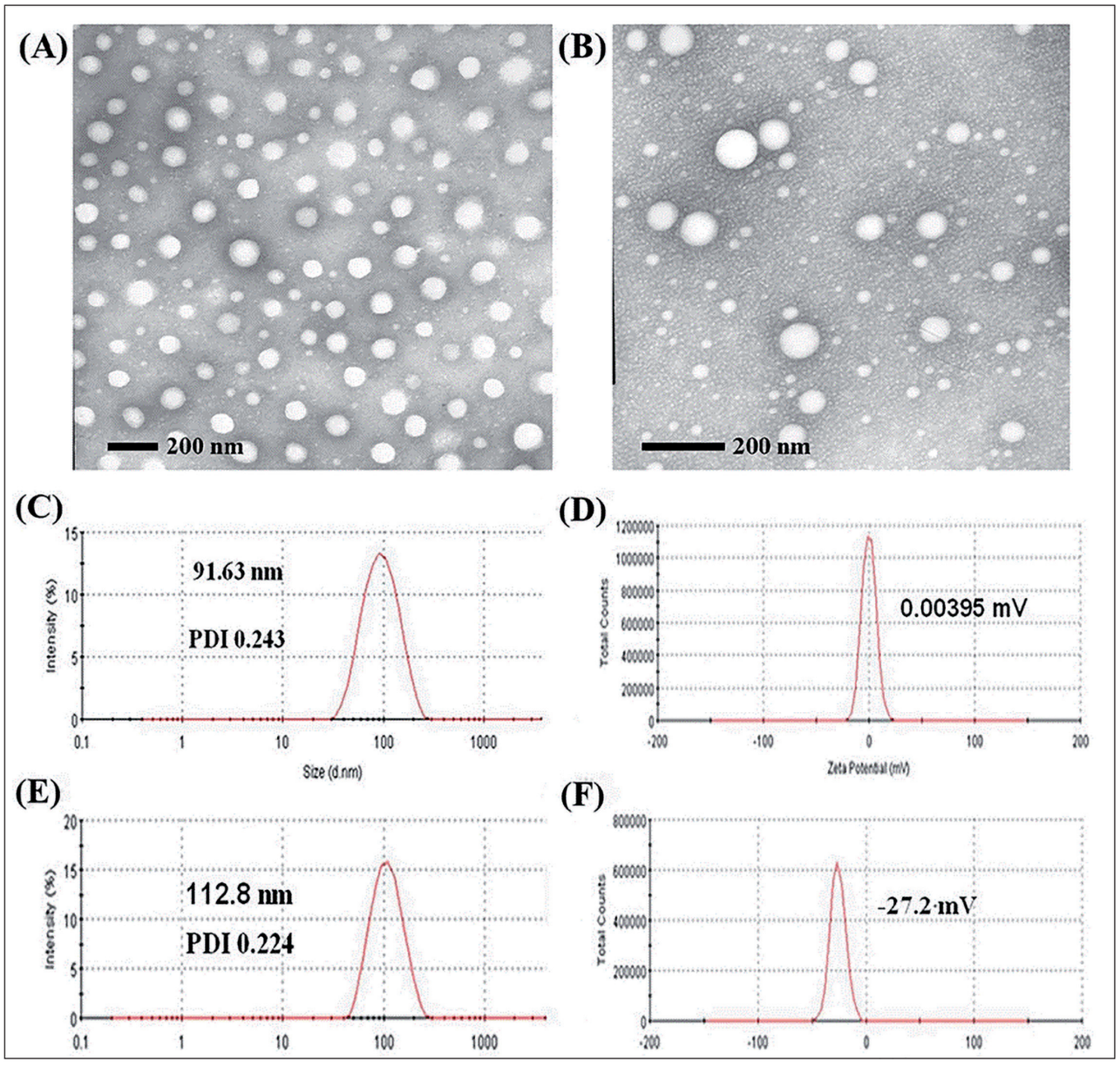

Fig. 2: TEM images of CHSP-SAN (A) and ADM-CHSP-SAN (B). Particle size distribution of CHSP-SAN (C) and ADM-CHSP-SAN (E). *Zeta* potential of CHSP-SAN (D) and ADM-CHSP-SAN (F).

was employed. The cytotoxicity assay demonstrated that the cell viability decreased gradually with the drug treatment time from 2 to 6 h. However, ADM-Sol and ADM-CHSP-SAN only caused less than 15 % of loss of cell viability after 4 h incubation (Fig. 4C). In order to evaluate the cytotoxicity of ADM-Sol and ADM-CHSP-SAN to C6 cells after crossing BBB *in vitro*, a concentration gradient of two ADM formulations were added into the upper chambers of transwells embedded dense HBMEC cell

Table 1: Models of release kinetic for ADM-CHSP-SAN

Model	pH 7.4	pH 6.8	pH 5.0
Zero order processes	Q=0.0101t+0.2131	Q=0.016t+0.2343	Q=0.0119t+0.3512
	R^2=0.8239	R^2=0.8155	R^2=0.7454
First order processes	ln(1-Q)=-0.0172t-0.2386	ln(1-Q)=-0.0191t-0.2657	ln(1-Q)=-0.029t-0.4371
	R^2=0.8867	R^2=0.8872	R^2=0.8601
Higuchi	$Q=0.0776t^{1/2}+0.1279$	$Q=0.0816t^{1/2}+0.1444$	$Q=0.0934t^{1/2}+0.2456$
	R^2=0.9592	R^2=0.9541	R^2=0.9124
Weibull	lnln(1/1-Q)=0.3711lnt-1.4755	lnln(1/1-Q)=0.3714lnt-1.3730	lnln(1/1-Q)=0.3665lnt-0.890
	R^2=0.9951	R^2=0.9693	R^2=0.9933

Q: fraction drug release; T: time; R^2: coefficient of correction.

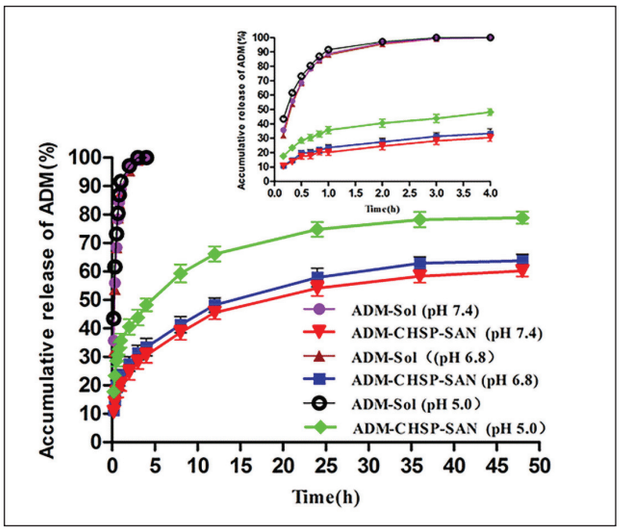

Fig. 3: *In vitro* release profiles of ADM-Sol and ADM-CHSP-SAN in pH 7.4, pH 6.8 and pH 5.0 release medium within 4 h (insert) and 48 h (n=3).

monolayer as BBB model for 4 h, and then the survival rate of C6 cells in the basolateral compartment for 48 h was detected by MTT assay. As shown in Fig. 4D, the IC_{50} of ADM-CHSP-SAN was 11.06±2.11 μM after crossing BBB *in vitro*. In contrast, the IC_{50} value of ADM-Sol was not detected in this experiment, indicating that the cytotoxicity of ADM-CHSP-SAN towards C6 cells was greater than ADM-Sol after penetrating the BBB *in vitro*.

2.4. *Cell apoptosis test*

To evaluate the C6 cells apoptosis the ADM-Sol or ADM-CHSP-SAN (equal to 5 μM of ADM) were added to the *in vitro* BBB model for 24 h. The results showed that ADM-Sol only induced 27.97±3.25 % of apoptotic C6 cells after across BBB *in vitro*, whereas ADM-CHSP-SAN induced 72.32±5.63% of apoptotic C6 cells (P<0.01) (Fig. 5). It may be account for the distinct penetration ability of ADM-Sol and ADM-CHSP-SAN when across BBB. Free ADM almost could not pass through the BBB (Tacar et al. 2013). On the contrary, CHSP-SAN may help ADM penetrate across the extracorporeal BBB through endocytosis and exocytosis effect (Han et al. 2018), and ultimately lead to high potent antitumor activity.

2.5. *Brain pharmacokinetic study*

Brain pharmacokinetic (B-PK) experiments were carried out by the B-MD technology, the *in vitro* and *in vivo* relative recovery of ADM were 32.35±0.76 % and 13.25±0.82 %, respectively. The B-PK profiles and parameters of two ADM formulations assessed with non-compartment model are exhibited in Fig. 6 and Table 2. The presented results on brain transport of ADM formulations showed that the peak time (T_{max}) of ADM-CHSP-SAN (i.n.) was significantly shorter than that of ADM-CHSP-SAN (i.v.) (P<0.01). The apparent volume of distribution (V_d) of drugs administered via the i.n. route was smaller than that after i.v. administration. The peak concentration (C_{max}) and area under the curve ($AUC_{0\text{-}12h}$) of ADM-CHSP-SAN administered i.n. were 1.59-fold and 1.53-fold greater than those given i.v. (P<0.01), respectively. The results implied that drugs may be primarily delivered into the brain through the direct nose-to brain pathway after i.n. administration, so higher drug concentration are reached in the brain (Illum 2000).

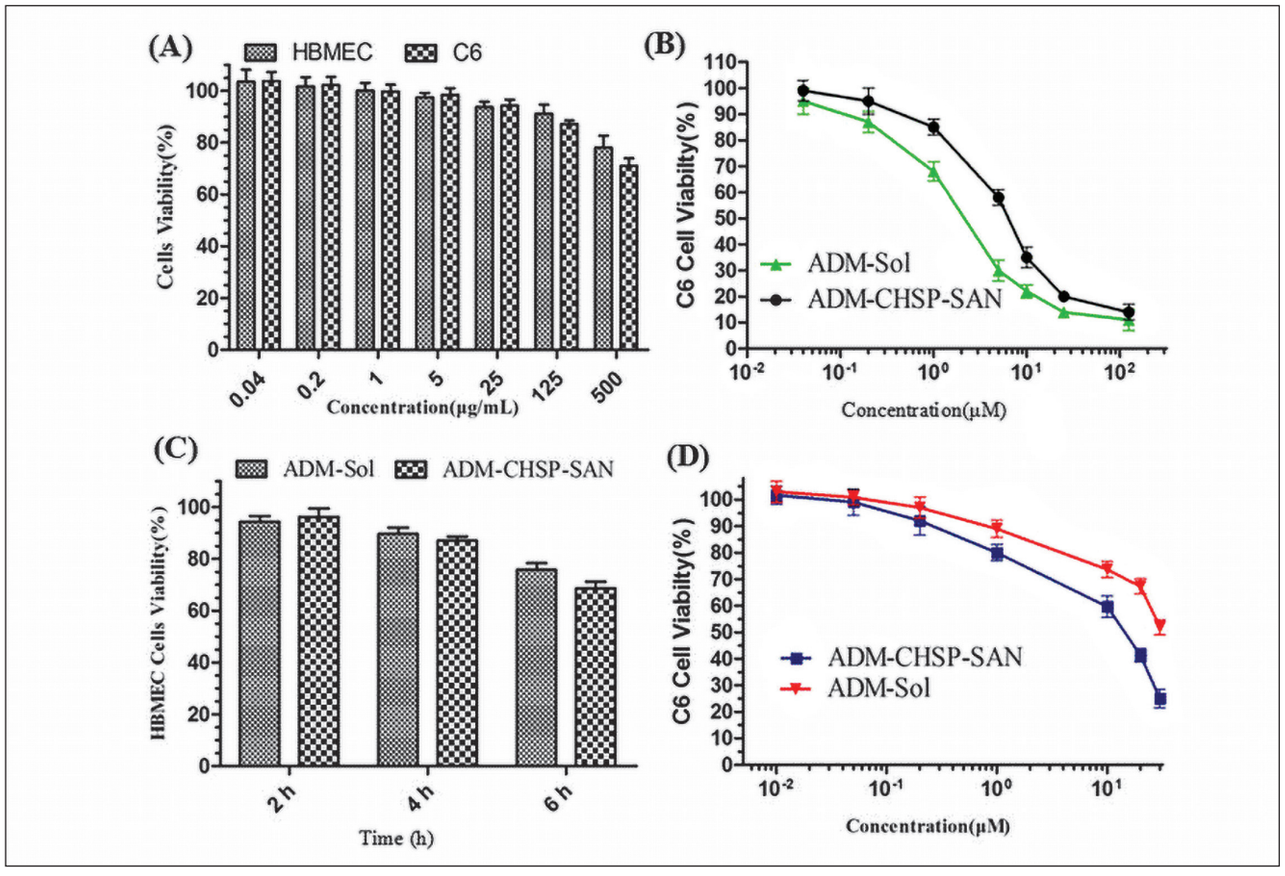

Fig. 4: Cell viability of C6 and HBMEC cells after being treated with medium containing CHSP-SAN at different concentrations (0.04~500 μg/mL) for 48 h (A). Cell viability of C6 cells after being treated with ADM-Sol and ADM-CHSP-SAN within a certain concentration range for 48 h (B). Cell viability of HBMEC cells after being treated with ADM-Sol and ADM-CHSP-SAN (30 μM) in 2, 4 and 6 h (C). Cell viability of C6 cells after being treated with ADM-Sol and ADM-CHSP-SAN within a certain concentration range after crossing BBB *in vitro* for 48 h (D).

Table 2: Pharmacokinetic parameters of ADM-CHSP-SAN and ADM-Sol in the brain of rats through *i.n.* administration and *i.v.* injection, mean±SD, n=5

Parameters	ADM-Sol		ADM-CHSP-SAN	
	i.v.	*i.n.*	*i.v.*	*i.n.*
$t_{1/2}$ (min)	382.26±27.68	271.70±35.42*	428.38±11.62$^{\#\#}$	354.9±24.46$^{\#\Delta\Delta}$
T_{max} (min)	60.21±8.87	10.35±1.00**	50.58±6.16$^{\#\#}$	29.96±2.21**$^{\#\#\Delta\Delta}$
C_{max} (μg/mL)	1.58±0.23	3.64±0.50**	2.71±0.35**	4.32±0.54**$^{\Delta\Delta}$
$AUC_{0\text{-}12h}$ (μg • min/mL)	310.09±45.42	350.54±47.84	541.07±35.73**$^{\#\#}$	826.22±100.53**$^{\#\#\Delta\Delta}$
$MRT_{0\text{-}\infty}$ (min)	292.91±29.67	329.28±37.98	468.60±17.77*$^{\#\#}$	454.95±36.41$^{\#}$
Vd (mg/kg/(μg/mL))	11.87±1.80	7.80±1.17*	6.70±1.00*	5.02±2.16*
CL(mg/kg/(μg/mL)/min)	0.021±0.003	0.020±0.004	0.01±0.02**$^{\#}$	0.008±0.001**$^{\#\#\Delta}$

*P <0.05, **P<0.01 vs ADM-Sol (*i.v.*) group; $^{\#}P$<0.05, $^{\#\#}P$<0.01 vs ADM-Sol (*i.n.*) group;
$^{\Delta}P$<0.05, $^{\Delta\Delta}P$<0.01 vs ADM-CHSP-SAN (*i.v.*) group.

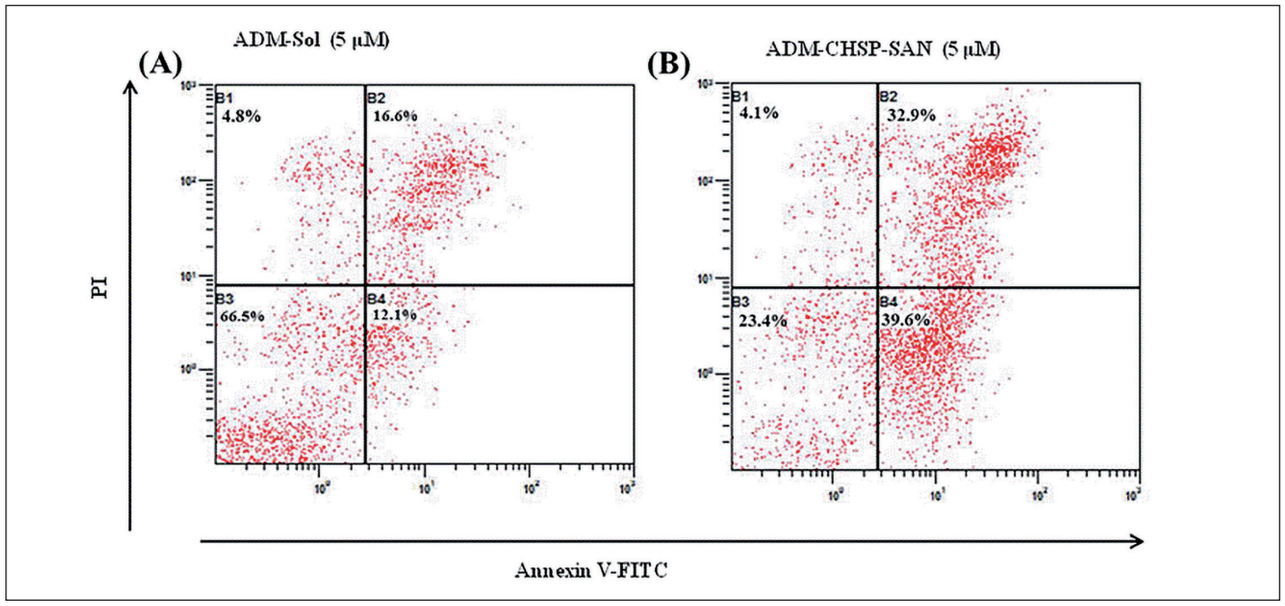

Fig. 5: Representative images of C6 cell apoptosis treatment with ADM-Sol (A) or ADM-CHSP-SAN (B) after crossing BBB *in vitro* for 24 h (staining with Annexin V/PI).

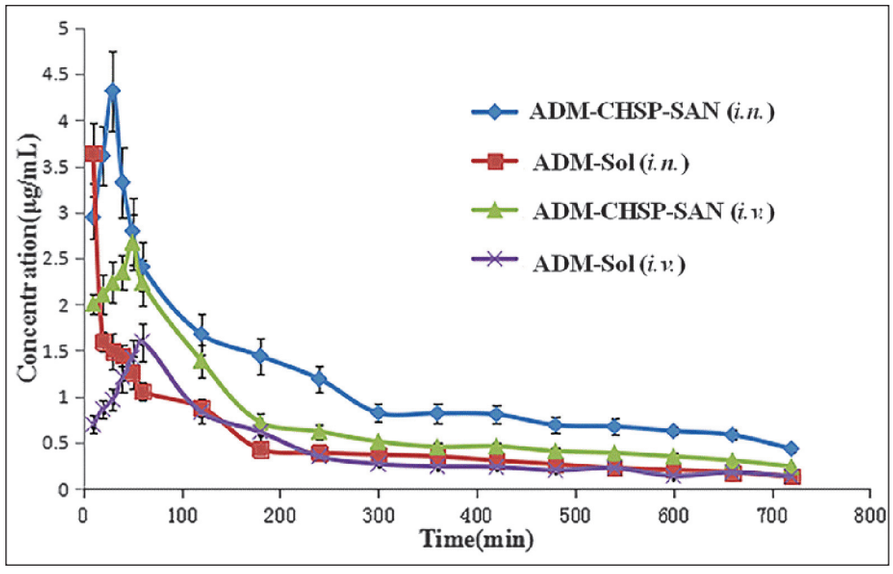

Fig. 6: Profiles of drug concentration-time in the hippocampus of rats (n=5).

Notably, the ratio of the AUC_{0-12h} between ADM-CHSP-SAN (i.n.) and ADM-Sol (i.n.) was significantly greater than that between ADM-CHSP-SAN (i.v.) and ADM solution (i.v.) (2.36 vs 1.74) (P<0.01). The $t_{1/2}$ and $MRT_{0-\infty}$ of ADM-CHSP-SAN (i.n.) was significantly prolonged (P<0.05), while the clearance rate (CL) was significantly reduced compared with the ADM-Sol (i.n.) group (P<0.01). The results demonstrated that ADM-CHSP-SAN circulate long and the ADM availability in the brain could be enhanced by nanoparticles delivery and intranasal administration. However, the T_{max} of ADM-Sol and ADM-CHSP-SAN was delayed to 60.21±8.87 min and 50.58±6.16 min after i.v. administration, respectively. ADM in the blood penetration into the brain is a slow process after intravenous administration. In the initial 60 min, the penetration rate of the drug into the brain was faster than its elimination rate, so the T_{max} appeared at around 60 min. In addition, ADM-CHSP-SAN in the brain has a certain sustained release, so the T_{max} of the nanodrug also had a certain delay. Similar phenomena were found in previous studies (Cheng et al. 2008; Chen et al. 2008; Pan et al. 2018).

3. Discussion

Among the biopolymers, pullulan based biomaterials are an ideal carriers to deliver drugs to the brain through the nasal-brain pathway for the following reasons: (1) pullulan is a natural non-ionic and linear homopolysaccharide with excellent biodegradability and low immunogenicity formed by repeating units of maltotriose condensed through α-1,6-linkages (Singh et al. 2008; Yang et al. 2014b), (2) pullulan-based nanoparticles were reported to adhere to the nasal epithelium (Grenha and Rodrigues 2013; Nochi et al. 2010) and (3) chemical modification was relatively easy, so pullulan has been considered platform material for drug delivery carriers (Scomparin et al. 2011; Zhang et al. 2011). Among these pullulan-based nanocarriers, the most common ones are cholesterol-modified pullulan nanoparticles being able to form polymeric nano-vehicles by self-aggregation and release drugs continuously (Yang et al. 2014a).

Apart from this, there are several crucial factors influencing the brain delivery efficiency of nasally applied nano-drug delivery systems. Gao et al. (2007) disclosed that nano-drugs at the size of 90-100 nm could automatically be concentrated in the olfactory mucosa, and directly delivered into the brain through endocytosis. It was also suggested that the drug should be lipophilic for better permeation through the nasal mucosa (Richter and Keipert 2004). We previously found that the size of SAN was scarcely affected by the concentration of CHSP in the range of 0.1~4.0 mg/mL, which implied that the particle interaction with SAN was almost negligible (Yang et al. 2010). Therefore, to achieve smaller particle sizes, better amphipathicity, higher EE% and DL%, as well as relatively enhanced permeation profile for intranasal nanocarriers, ADM-CHSP-SAN was selected as the final optimized formulation to transport drugs into the brain. Besides, the negatively charged surface of nanoparticles would exhibit a potential long-circulating property because of the realization that these features could reduce plasma protein adsorption and nonspecific cellular uptake (Alexis et al. 2008; Yamamoto et al. 2001). Therefore, ADM-CHSP-SAN with negatively charge would have a long-circulating action.

In addition to the sustained release phenomenon, we observed that ADM released from CHSP-SAN exhibited a significant decreasing in the release rate along with the increasing pH in medium. It is known that the release rate of a drug incorporated in a hydrophobic domain depends on the drug solubility and diffusion velocity. This pH-responsive manner of ADM release might assist the quick diffusion of ADM from the acidic endosome/lysosome and intracellular transfer into the nucleus and enhanced the antitumor effect of the drug (Xu et al. 2016).

Our previous studies indicated that free ADM showed a higher uptake rate in C6 glioma cells compared with the ADM-loaded nanoparticles *in vitro* and resulted in significantly higher cytotoxicity with lower IC_{50} value (Xu et al. 2016). However, when the BBB existed, the cytotoxicity of the two formulations to C6 cells were reversed. ADM-CHSP-SAN were capable of inducing a significantly higher proportion of apoptotic cells than ADM-Sol after across the BBB (P<0.01). This result was consistent with the literature which demonstrated the pullulan based DDS could undergo cellular endocytosis via clathrin or raft/caveolae dependent endocytosis (Thomsen et al. 2011). In addition, ADM loaded CHSP-SAN exhibited higher cytotoxicity that may be attributed to enhance interaction with cells as well as the rapid release of ADM triggered by tumor pH (Na et al. 2000).

Intranasal drug administration has developed as a valuable tool to target therapeutics to the brain for its advantages of non-invasive, and BBB bypassing (Dhuria et al. 2010; Hanson and Frey 2008). To further evaluate the nose-to-brain targeting ability of ADM-CHSP-SAN via the intranasal route, we investigated the brain pharmacokinetic profiling of ADM loaded nanocarriers by the B-MD technology, a promising method for studying drug delivery to the CNS in laboratory and clinic (Dave et al. 2013; Neumann et al. 2013; Portnow et al. 2017). Considering the rapid mucociliary clearance, awake animals were suggested to avoid the anaesthetic agents which may induce mucociliary clearance alteration during pharmacokinetic studies (Mayor and Illum 1997). Therefore, B-MD was applied to study the brain pharmacokinetics after i.n. administration in this study.

The pathways mediating drug absorption through the nasal mucosa mainly were the olfactory nerve pathway, the olfactory mucosa epithelium pathway and the blood circulation pathway (Illum 2000). It is known that the olfactory pathway consprises the hippocampus, etc. The B-PK results showed that the drug was generally localized in higher amounts in the hippocampus of the brain after i.n. administration, indicating that the drug predominantly followed the olfactory route of drug delivery to the CNS (Babu et al. 2011). In view of the *in vitro* cytotoxicity study, the transport mechanism across the BBB might be ascribed to cellular endocytosis via clathrin or raft/caveolae dependent endocytosis (Thomsen et al. 2011). Therefore it could be deduced that there was an effect of direct transport in the olfactory nerve pathway.

Taken together, the rapid and continuous delivery of ADM-CHSP-SAN into the brain was mainly co-mediated by the olfactory nerve pathway and the olfactory mucosa epithelium pathway. Therefore, higher drug concentrations in the brain were reached faster than with ADM-CHSP-SAN (i.v.) and ADM-Sol (i.v.). The lack of absorption phase of ADM-Sol (i.n.) compared with other groups suggested that i.n. administration could transport free drugs into the brain fast. Lipophilicity could also facilitate partly passive diffusion across the BBB (Chen et al. 2008). Besides, after i.v. administration, the AUC_{0-12h} of ADM-CHSP-SAN was higher than ADM-Sol, suggesting that CHSP-SAN could promote crossing the BBB rapidly through the blood circulation pathway (Pan et al. 2018). However, which pathway plays the most important role in delivering ADM-CHSP-SAN into the brain, needs further studies.

In this study, the B-PK results implied that the ADM availability in the brain could be enhanced by CHSP-SAN via i.n. administration. The findings were consistent with our previous study, in which we demonstrated that PLA nanoparticles and chitosan modified PLA nanoparticles showed a potential for improving the efficacy of the direct nose-to-brain transport for drugs (Cheng et al. 2008; Zhang et al. 2013). The ability of pullulan-based nanocarriers adhering to the surfaces of nasal mucosa cells might improve the carriers' MRT and enhance the encapsulated drug absorption (Grenha and Rodrigues 2013). As a result, the $t_{1/2}$ and $MRT_{0-\infty}$ of ADM-CHSP-SAN (i.n.) was greatly prolonged (P<0.05), while the clearance rate (CL) was significantly reduced compared with the ADM-Sol (i.n.) group (P<0.01). This may benefit from the negatively charged surface of nanoparticles and the sustained drugs release in the brain. This feature was also demonstrated by many other investigators. Gao et al. found that nanoparticles coated with Polysorbate 80 could greatly enhance drug delivery into both the brain tissues and cerebrospinal fluids after i.v. administration compared to uncoated ones and simple solutions (Gao and Jiang 2006).

In conclusion, we successfully constructed ADM-CHSP-SAN as sustained release and brain targeting nanoparticles. CHSP-SAN

showed good biocompatibility, and ADM loaded CHSP-SAN showed a better inhibition activity on C6 cells after crossing BBB *in vitro*. Importantly, the B-PK study conducted by B-MD technology showed that the brain targeting effects of ADM could be enhanced by CHSP-SAN via i.n. administration. ADM-CHSP-SAN reduced the CL, prolonged $MRT_{0-\infty}$ and significantly increased ADM availability, probably due to the favored BBB bypassing of CHSP-SAN and the direct transport from the nose-to-brain through the olfactory and trigeminal nerves. In this work, we presented a novel non-invasive strategy for intranasal delivery of pullulan-based nanocarriers which may greatly enhance the transport of small molecular drugs into the brain.

4. Experimental

4.1. Materials

Pullulan (Mw=200,000) was purchased from Hayashibara (Tokyo, Japan). Cholesterol was purchased from Dingguo Changsheng Co.Ltd. (Beijing, China). Adriamycin hydrochloride (ADM-HCL) was kindly gifted by Haizheng Pharmaceutical Co. (Hangzhou, China). Penicillin, streptomycin, DMEM, D-Hank's buffer solution, fetal bovine serum (FBS) and 0.25% (w/v) trypsin solution were purchased from Gibco BRL (Gaithersberg MD, USA). 3-(4,5-Dimethylthizol-2-yl)-2,5-diphenyltetrazolium bromide (MTT), and dimethyl sulfoxide (DMSO) were obtained from Sigma-Aldrich Co. Ltd. (St. Louis, MO, USA). Other chemicals and solvents were all of analytical grade, and purified water was produced by a Millipore® water purification system.

4.2. Cells and animals

HBMEC, C6 glioma cell line and Wistar rats (200±20 g, male) were supplied by the Laboratory Animal Centre, Zhejiang Chinese Medical University (Hangzhou, China). All the experiments were performed in accordance with the Ethical Committee for the USE of Laboratory Animals of Zhejiang Chinese Medical University.

4.3. Preparation of CHSP-SAN

CHSP, with a degree of substitute of 5.20 cholesterol residues per 100 glucose units in pullulan, was synthesized according to the literatures (Yang et al. 2010). CHSP-SAN were prepared by a probe sonication method (Yang et al. 2014a). Briefly, CHSP conjugates (15 mg) were suspended and swollen in deionized water under gentle shaking at 37 °C for 24 h to gain a milky suspension (CHSP-SAN), followed by pulse-sonication (pulse on 2.0 s, pulse off 2.0 s) at 50 W for 2 min in ice-water bath. The solution of CHSP-SAN was filtrated (pore size: 0.45 μm, Millipore®) and stored at 4 °C.

4.4. ADM loading

ADM was loaded into the CHSP-SAN by a dialysis method (Cui et al. 2013). Briefly, ADM-HCL was dissolved in DMSO, mixed with 3-fold molar excess of triethylamine (TEA) and stirred overnight. Then 1 mg/mL ADM-Sol was added to CHSP-SAN solution dropwise and stirred for 12 h in the dark. After completing the reaction, the mixture was filtered and dialysed against deionized water to remove free ADM (MWCO=8~14 kDa). The dialyzed solution containing ADM-CHSP-SAN was freeze-dried and subjected to further investigation.

4.5. Characterization of CHSP-SAN and ADM-CHSP-SAN

The size, PDI and *zeta* potential of CHSP-SAN and ADM-CHSP-SAN were determined by dynamic light scattering (DLS, Malvern Nano-ZS90, UK) at 25 °C. Morphological observation was performed on the TEM (HT7700, Hitachi, Japan). The EE% and DL% of ADM in carriers were determined by UV-visible scanning spectrophotometer (SHIMADZU UV-1700, Japan) at 482 nm.

4.6. In vitro release study

In order to examine the release characteristics of ADM-CHSP-SAN under different conditions *in vitro* and to investigate whether the nanodrug has sustained and low pH sensitive drug release characteristics, three pH gradients (pH 7.4, pH 6.8 and pH 5.0) were used. ADM release behaviors from CHSP-SAN were investigated by a dialysis bag method as described in the literature (Gasparini et al. 2008). Briefly, 2 mL of ADM-CHSP-SAN solution were placed inside a dialysis bag (MWCO=8~14 kDa), which was immersed in PBS (25 mL, pH 7.4, pH 6.8 and pH 5.0) and incubated at 37±0.2 °C in an air-bath shaker at 100 rpm. At predetermined time intervals, samples were withdrawn and replaced with an equal volume of fresh media. The release manner of free ADM was performed in the same condition as a control. The ADM concentrations were measured by UV-visible scanning spectrophotometer at 482 nm (Yang et al. 2014a). The *in vitro* release study was carried out for 48 h. All tests were carried out in triplicate.

4.7. Cell culture

HBMEC were cultured in DMEM cell culture medium containing 20% fetal bovine serum, endothelial cell growth factor (ECGF, 100 μg/mL), L-glutamine (2 mM), heparin (20 μg/mL), insulin (40 μU/mL), penicillin (100 U/mL), streptomycin (100 U/mL). C6 glioma cells were cultured in the DMEM cell culture medium containing 10% fetal bovine serum, penicillin (100 U/mL), streptomycin (100 U/mL). Cells were incubated at 37 °C with 5% CO_2.

4.8. In vitro cytotoxicity assay

The cytotoxicity of CHSP-SAN on both HBMEC and C6 cells, and cytotoxicity of ADM-CHSP-SAN and ADM-Sol on C6 cells were evaluated. Briefly, cells under exponential phase were seeded in 96-well plates with a density of 5×10^3 cells/well in 200 μL growth medium and grown overnight. Then cells were treated with CHSP-SAN (0.04~500 μg/mL) or ADM formulations (ADM-Sol and ADM-CHSP-SAN) at a concentration range of ADM from 0.04 to 125 μM in culture medium. After 48 h incubation, all media were replaced by fresh culture medium containing MTT solution (0.5 mg/mL). After additional incubation for 4 h, all media were replaced by DMSO. The OD values were measured by a microplate reader (Spectra Max M3, Molecular Devices, USA) at 570 nm, and cell viability was calculated by dividing the OD values of samples with the OD values of blank. All the experiments were repeated three times independently.

In order to determine the BBB penetration ability and the cytotoxicity of the ADM-CHSP-SAN, we constructed an *in vitro* BBB model described previously (Han et al. 2018). Briefly, HBMEC were seeded into the transwell inserts (Polycarbonate Membrane Transwell Inserts of 3 μm mean pore size, Corning, NY, USA) at a density of 10^5 cells/well and the culture medium was replaced every two days. The integrity of the BBB model was assessed according to the transendothelial electrical resistance (TEER) value greater than 200 Ω/cm^2 (Millicell-RES, Millipore®, USA). Then, the C6 cells were seeded in 12-well plates at a density of 2.5 x 10^4 cells/well and incubated for 24 h as the acceptor compartments (downer wells). Then all transwell inserts with constructed BBB model were placed to each 12-well plate, and ADM-Sol and ADM-CHSP-SAN were added at a concentration range of ADM from 0.01 to 30 μM into each corresponding upper insert respectively and incubated for another 4 h. The viability of C6 cells in the acceptor compartments was calculated by MTT method after 48 h incubation.

4.9. Cell apoptosis test

ADM-Sol or ADM-CHSP-SAN (equal to 5 μM of ADM) were added to the upper chambers of transwells embedded the *in vitro* BBB model and incubated for 4 h, then the C6 cells in the basolateral compartments were incubated for additional 24 h. All C6 cells were harvested and conducted to detect the apoptosis using an Annexin V-FITC/PI staining kit (BD Bioscience, USA) following the manufacturer's protocol. The percentage of apoptotic cells was determined and then analyzed by a Guava Easy Cytometer (Guava Technologies, Merck Drugs & Biotechnology, Germany) within 1 h.

4.10. Brain pharmacokinetic study

4.10.1. Surgical procedures

Wistar rats were anesthetized with 3% pentobarbital (45 mg/kg) by intraperitoneal injection and mounted on a brain stereotactic apparatus (Bioanalytical Systems, West Lafayette, IN, USA). The surgical procedure was described previously (Bergquist et al. 1996). Briefly, one hole (0.5 mm diameter) was drilled through the skull by a trephine drill at hippocampus (AP:-4.8, ML:-5.0 from the bregma and DV:-4.0 from the dura). Anintracerebral guide cannula (MD-2251, BAS, West Lafayette, IN, USA) with styles was stereotaxically implanted and fixed with skull screws and dental acrylic cement (Paxinos and Watson 1996). The animals were allowed to recover with free access to food and water for 24 h before agent administration.

4.10.2. Recovery determination

In B-MD studies, the *in vitro* or *in vivo* B-MD recovery of ADM is usually determined by retrodialysis method (Babu et al. 2011). The *in vitro* recovery by gain was tested by placing B-MD probes (MD-2200, BAS, USA) in ADM (5 μg/mL or 10 μg/mL or 25 μg/mL) of modified Ringer's solution and perfusing the fluid at 2 μL/min. The samples were collected from each probe at 10 min intervals after initial equilibration for 20 min. The recovery *in vitro* was calculated as:

$$Relative\ recovery_{(in\ vivo)} = \frac{C_{dialysate}}{C_{medium} - C_{dialysate}} \quad (1)$$

The *in vivo* recovery of ADM by loss was determined by implanting B-MD probes in the hippocampus as described in the previous sections. Blank modified Ringer's solution was perfused through the probes after implantation at 2 μL/min. Then the perfusate was changed to ADM (5 μg/mL or 10 μg/mL or 25 μg/mL) of modified Ringer's solution, and the dialysates were collected every 10 min for 60 min. The recovery *in vivo* was calculated as:

$$Relative\ recovery_{(in\ vivo)} = \frac{C_{perfuse} - C_{dialysate}}{C_{perfusate}} \quad (2)$$

All the samples were collected three times independently for each ADM concentration, and then analyzed through a high performance liquid chromatography (HPLC) instrument (Agilent Technologies Co. Ltd., USA).

4.10.3. Brain pharmacokinetic study of ADM-CHSP-SAN

All rats were randomly divided into four groups (n=5), and the ADM-Sol or ADM-CHSP-SAN were injected into the tail vein or into the nasal cavity of the

right nostril by a home-made patent device at a dosage of 8 mg/kg body weight. All microdialysis experiments were performed in freely moving animals kept in an awake animal caging system (Stand-Alone Return and Rodent Bowl kit, BAS, West Lafayette, IN, USA). Microdialysate samples were collected at each predetermined interval up to 12 h duration and then analyzed through HPLC.

4.11. Data analysis

Data was expressed as mean±standard deviations (SD). Significant differences in the mean values were evaluated by one-way analysis of variance (ANOVA). Pharmacokinetic modeling and pharmacokinetic parameter estimations were carried out by Winnonlin-5.2 software. A statistical test with a *P* value less than 0.05 or 0.01 was considered significant.

Acknowledgement: This study was financially supported by General Research Project of Zhejiang Provincial Education Department (No.Y201431480), Traditional Chinese Medicine Science and Technology Plan of Zhejiang Province (No.2018ZQ012, No.2018ZQ013), Opening Project of Zhejiang Provincial First-rate Subject (Chinese Traditional Medicine), Zhejiang Chinese Medical University (No.Ya2017007) and National Natural Science Foundation of China (No.81473361, No.81673607).

Conflicts of interest: None reported.

References

Alexis F, Pridgen E, Molnar LK, Farokhzad OC (2008) Factors affecting the clearance and biodistribution of polymeric nanoparticles. Mol Pharm 5**:** 505-515.

Babu RJ, Dayal PP, Pawar K, Singh M (2011) Nose-to-brain transport of melatonin from polymer gel suspensions: a microdialysis study in rats. J Drug Target 19**:** 731-740.

Bergquist J, Vona MJ, Stiller C, O'Connor WT, Falkenberg T, Ekman R (1996) Capillary electrophoresis with laser-induced fluorescence detection: a sensitive method for monitoring extracellular concentrations of amino acids in the periaqueductal grey matter. J Neurosci Meth 65**:** 33-42.

Bharali DJ, Klejbor I, Stachowiak EK, Dutta P, Roy I, Kaur N, Bergey EJ, Prasad PN, Stachowiak MK (2005) Organically modified silica nanoparticles: a nonviral vector for in vivo gene delivery and expression in the brain. P Natl Acad Sci USA 102**:** 11539-11544.

Carlan IC, Estevinho BN, Rocha F (2017) Study of microencapsulation and controlled release of modified chitosan microparticles containing vitamin B12. Powder Technology 318**:** 162-169.

Chen J, Wang X, Wang J, Liu G, Tang X (2008) Evaluation of brain-targeting for the nasal delivery of ergoloid mesylate by the microdialysis method in rats. Eur J Pharm Biopharm 68**:** 694-700.

Cheng Q, Feng J, Chen J, Zhu X, Li F (2008) Brain transport of neurotoxin-I with PLA nanoparticles through intranasal administration in rats: a microdialysis study. Biopharm Drug Dispos 29**:** 431-439.

Clementino A, Batger M, Garrastazu G, Pozzoli M, Del Favero E, Rondelli V, Gutfilen B, Barboza T, Sukkar M, Souza S, Cantù L, Sonvico F (2016) The nasal delivery of nanoencapsulated statins - an approach for brain delivery. Int J Nanomed 11**:** 6575-6590.

Cui C, Xue Y, Wu M, Zhang Y, Yu P, Liu L, Zhuo R, Huang S (2013) Cellular uptake, intracellular trafficking, and antitumor efficacy of doxorubicin-loaded reduction-sensitive micelles. Biomaterials 34**:** 3858-3869.

Dave N, Gudelsky GA, Desai PB (2013) The pharmacokinetics of letrozole in brain and brain tumor in rats with orthotopically implanted C6 glioma, assessed using intracerebral microdialysis. Cancer Chemoth Pharm 72**:** 349-357.

De Lange EC (2013) The mastermind approach to CNS drug therapy: translational prediction of human brain distribution, target site kinetics, and therapeutic effects. Fluids Barriers CNS 10**:** 12-12.

Dhuria SV, Hanson LR, Frey WH II (2010) Intranasal delivery to the central nervous system: mechanisms and experimental considerations. J Pharm Sci 99**:** 1654-1673.

Gao J, Fang L, Sun D, Shen Y, Hu Y, Li N, Chang J, Li W, Tan J (2016) 131I-labeled and DOX-loaded multifunctional nanoliposomes for radiotherapy and chemotherapy in brain gliomas. Brain Res doi**:** 10.1016/j.brainres.2016.12.014.

Gao K, Jiang X (2006) Influence of particle size on transport of methotrexate across blood brain barrier by polysorbate 80-coated polybutylcyanoacrylate nanoparticles. Int J Pharm 310**:** 213-219.

Gao X, Wu B, Zhang Q, Chen J, Zhu J, Zhang W, Rong Z, Chen H, Jiang X (2007) Brain delivery of vasoactive intestinal peptide enhanced with the nanoparticles conjugated with wheat germ agglutinin following intranasal administration. J Control Release 121**:** 156-167.

Gasparini G, Kosvintsev SR, Stillwell MT, Holdich RG (2008) Preparation and characterization of PLGA particles for subcutaneous controlled drug release by membrane emulsification. Colloid Surface B 61**:** 199-207.

Gloor SM, Wachtel M, Bolliger MF, Ishihara H, Landmann R, Frei K (2001) Molecular and cellular permeability control at the blood-brain barrier. Brain Res Rev 36**:** 258-264.

Grenha A, Rodrigues S (2013) Pullulan-based nanoparticles: future therapeutic applications in transmucosal protein delivery. Ther Deliv 4**:** 1339-1341.

Guo X, Zheng H, Guo Y, Wang Y, Anderson G, Ci Y, Yu P, Geng L, Chang Y (2017) Nasal delivery of nanoliposome-encapsulated ferric ammonium citrate can increase the iron content of rat brain. J Nanobiotechnol 15**:** 42-55.

Han S, Zheng H, Lu Y, Sun Y, Huang A, Fei W, Shi X, Xu X, Li J, Li F (2018) A novel synergetic targeting strategy for glioma therapy employing borneol combination with angiopep-2-modified, DOX-loaded PAMAM dendrimer. J Drug Target 26**:** 86-94.

Hanson LR, Frey WH II (2008) Intranasal delivery bypasses the blood-brain barrier to target therapeutic agents to the central nervous system and treat neurodegenerative disease. Bmc Neurosci 9**:** S5.

Hefnawy A, Khalil IA, El-Sherbiny IM (2017) Facile development of nanocomplex-in-nanoparticles for enhanced loading and selective delivery of doxorubicin to brain. Nanomedicine 12**:** 2737-2761.

Illum L (2000) Transport of drugs from the nasal cavity to the central nervous system. Eur J Pharm Sci 11**:** 1-18.

Illum L (2002) Nasal drug delivery: new developments and strategies. Drug Discov Today 7**:** 1184-1189.

Li F, Feng J, Cheng Q, Zhu W, Jin Y (2007) Delivery of 125I-cobrotoxin after intranasal administration to the brain: a microdialysis study in freely moving rats. Int J Pharm 328**:** 161-167.

Mayor SH, Illum L (1997) Investigation of the effect of anaesthesia on nasal absorption of insulin in rats. Int J Pharm 149**:** 123-129.

Meng J, Agrahari V, Ezoulin MJ., Zhang C, Purohit SS, Molteni A, Dim D, Oyler NA., Youan B-BC (2016) Tenofovir containing thiolated chitosan core/shell nanofibers: in vitro and in vivo evaluations. Mol Pharm 13**:** 4129-4140.

Na K, Park KH, Kim SW, Bae YH (2000) Self-assembled hydrogel nanoparticles from curdlan derivatives: characterization, anti-cancer drug release and interaction with a hepatoma cell line (HepG2). J Control Release 69**:** 225-236.

Neumann ID, Maloumby R, Beiderbeck DI, Lukas M, Landgraf R (2013) Increased brain and plasma oxytocin after nasal and peripheral administration in rats and mice. Psychoneuroendocrinol 38**:** 1985-1993.

Nochi T, Yuki Y, Takahashi H, Sawada S, Mejima M, Kohda T, Harada N, Kong IG, Sato A, Kataoka N, Tokuhara D, Kurokawa S, Takahashi Y, Tsukada H, Kozaki S, Akiyoshi K, Kiyono H (2010) Nanogel antigenic protein-delivery system for adjuvant-free intranasal vaccines. Nat Mater 9**:** 572-578.

Pan L, Zhou J, Ju F, Zhu H (2018) Intranasal delivery of alpha-asarone to the brain with lactoferrin-modified mPEG-PLA nanoparticles prepared by premix membrane emulsification. Drug Deliv Trasnsl Re 8: 83-96.

Pardridge WM (2005) The blood-brain barrier: bottleneck in brain drug development. NeuroRx 2**:** 3-14.

Paxinos G, Watson L (eds) (1996) The rat brain in stereotaxic coordinates, 3rd edn.

Portnow J, Synold TW, Badie B, Tirughana R, Lacey SF, D'Apuzzo M, Metz MZ, Najbauer J, Bedell V, Vo T, Gutova M, Frankel P, Chen M, Aboody KS (2017) Neural stem cell-based anticancer gene therapy: a first-in-human study in recurrent high-grade glioma patients. Clin Cancer Res 23**:** 2951-2960.

Potter WZ (2012) New era for novel CNS drug development. Neuropsychopharmacol 37**:** 278-280.

Rekha MR, Sharma CP (2011) Hemocompatible pullulan-polyethyleneimine conjugates for liver cell gene delivery: In vitro evaluation of cellular uptake, intracellular trafficking and transfection efficiency. Acta Biomater 7**:** 370-379.

Richter T, Keipert S (2004) In vitro permeation studies comparing bovine nasal mucosa, porcine cornea and artificial membrane: androstenedione in microemulsions and their components. Eur J Pharm Biopharm 58**:** 137-143.

Scomparin A, Salmaso S, Bersani S, Satchi-Fainaro R, Caliceti P (2011) Novel folated and non-folated pullulan bioconjugates for anticancer drug delivery. Eur J Pharm Sci 42**:** 547-558.

Shen S, Li H, Yang W (2014) The preliminary evaluation on cholesterol-modified pullulan as a drug nanocarrier. Drug Deliv 21**:** 501-508.

Simakov SA, Tsur Y (2007) Surface stabilization of nano-sized titanium dioxide: improving the colloidal stability and the sintering morphology. J Nanopart Res 9**:** 403-417.

Singh RS, Saini GK, Kennedy JF (2008) Pullulan: Microbial sources, production and applications. Carbohyd Polym 73**:** 515-531.

Tacar O, Sriamornsak P, Dass CR (2013) Doxorubicin: an update on anticancer molecular action, toxicity and novel drug delivery systems. J Pharm Pharmacol 65**:** 157-170.

Thomsen LB, Lichota J, Kim KS, Moos T (2011) Gene delivery by pullulan derivatives in brain capillary endothelial cells for protein secretion. J Control Release 151**:** 45-50.

Xu X, Li J, Han S, Tao C, Fang L, Sun Y, Zhu J, Liang Z, Li F (2016) A novel doxorubicin loaded folic acid conjugated PAMAM modified with borneol, a nature dual-functional product of reducing PAMAM toxicity and boosting BBB penetration. Eur J Pharm Sci 88**:** 178-190.

Yamamoto Y, Nagasaki Y, Kato Y, Sugiyama Y, Kataoka K (2001) Long-circulating poly(ethylene glycol)-poly(d,L-lactide) block copolymer micelles with modulated surface charge. J Control Release 77**:** 27-38.

Yang W, Chen H, Gao F, Chen M, Li X, Zhang M, Zhang Q, Liu L, Jiang Q, Wang Y (2010) Self-aggregated nanoparticles of cholesterol-modified pullulan conjugate as a novel carrier of mitoxantronep. Curr Nanosci 6**:** 298-306.

Yang W, Wang M, Ma L, Li H, Huang L (2014a) Synthesis and characterization of biotin modified cholesteryl pullulan as a novel anticancer drug carrier. Carbohyd Polym 99**:** 720-727.

Yang X, Niu Y, Zhao N, Mao C, Xu F (2014b) A biocleavable pullulan-based vector via ATRP for liver cell-targeting gene delivery. Biomaterials 35**:** 3873-3884.

Zhang H, Li F, Yi J, Cu C, Fan L, Qiao Y, Tao Y, Cheng C, Wu H (2011) Folate-decorated maleilated pullulan-doxorubicin conjugate for active tumor-targeted drug delivery. Eur J Pharm Sci 42**:** 517-526.

Zhang X, Liu L, Chai G, Zhang X, Li F (2013) Brain pharmacokinetics of neurotoxin-loaded PLA nanoparticles modified with chitosan after intranasal administration in awake rats. Drug Dev Ind Pharm 39**:** 1618-1624.